Journal of Medicinal Chemistry

pubs.acs.org/jmc

Article

Design, Synthesis, and Evaluation of a Novel ^{99m}Tc-Labeled Small Molecule Inhibitor (Lapatinib)-Based SPECT Tracer Targeting HER2

Zuojie Li, Lina Diao, Peiwen Han, Qingna Xiao, Dajie Ding, Junhong Feng, Jianyong Jiang,* and Junbo Zhang*

Cite This: *J. Med. Chem.* 2025, 68, 23620−23631

Read Online

ACCESS | Metrics & More | Article Recommendations | Supporting Information

ABSTRACT: Radiolabeled human epidermal growth factor receptor 2 (HER2) tracers are important tools for the accurate clinical diagnosis and treatment of HER2-positive tumors. The aim of this study was to investigate the potential of small molecule inhibitors (lapatinib) as target groups for novel radiotracers targeting HER2. Twelve stable radiotracers were prepared by chelation with different coligands. The relationships between the linker and the combination of coligands with pharmacodynamics were systematically evaluated. [^{99m}Tc]Tc-Lapa-HYNIC-TPPTS exhibits the most favorable pharmacokinetic properties, as it can stably bind to the active pocket of the HER2 protein. Both *in vitro* and *in vivo* studies demonstrated its high targeting specificity toward HER2. SPECT images of [^{99m}Tc]Tc-Lapa-HYNIC-TPPTS in HER2-positive model mice revealed that it can effectively locate tumors. This study is the first attempt at a ^{99m}Tc-labeled small-molecule inhibitor tracer targeting HER2, showing great potential for applications in the diagnosis of HER2-positive cancers.

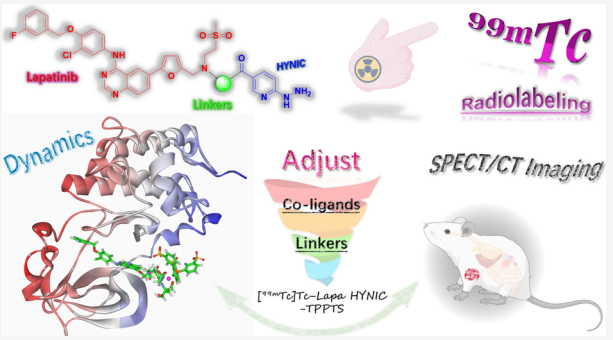

INTRODUCTION

Human epidermal growth factor receptor 2 (HER2) is a tyrosine kinase-active transmembrane receptor-like protein encoded by the c-erbB-2 gene located on chromosome 17q21.[1−3] It is one of the members of the epidermal growth factor receptor (EGFR) family and is expressed to varying degrees in various tumor tissues. HER2 is one of the earliest discovered "oncogenes" and due to its impact on cell proliferation, migration, invasion, and survival, it is often associated with poor prognosis and has become one of the most important targets in cancer research and treatment fields.[4−7]

Effective assessment of HER2 expression levels is key for accurate screening of patients with HER2-positive tumors and the development of individualized treatment plans.[8−10] Currently, the detection of HER2 overexpression generally involves taking biopsy samples for pathological examination. The main methods of examination are immunohistochemical staining and fluorescence *in situ* hybridization.[11,12] However, this invasive test cannot be repeated as a routine check for tumor efficacy evaluation. In addition, HER2 overexpression is heterogeneous within and between tumors, indicating that HER2 expression may differ within a primary tumor, between primary and metastatic lesions, and even within different metastatic sites.[13,14] HER2 expression may also change during the treatment of lesions. The complexity and variability in time and space make accurate detection difficult.[8,15]

Radiotracers provide noninvasive information at the molecular and cellular level and can be combined with nuclear imaging equipment to provide a comprehensive and visual view of HER2 expression in all tumors (primary tumors, lymph node metastases, and distant metastases) in the body in a single examination.[16,17] This provides key information for accurate clinical diagnosis and treatment and has become an important tool in precision medicine. Targeted HER2 radiotracers have been extensively studied and are broadly classified into five categories: monoclonal antibodies (e.g., [^{89}Zr]Zr-Df/DFO),[18,19] nanobodies (e.g., [^{68}Ga]Ga-NOTA-2Rs15d),[20] affinity substrates (e.g., [^{68}Ga/^{111}In]Ga/In-DOTA-$(HE)_3$-ADAPT6),[21] specific peptides (e.g., [^{99m}Tc]Tc-HP-Ark2)[22] and small-molecule inhibitors (e.g., [^{11}C]Tucatinib).[23] In clinical research, these radiotracers have shown preliminary potential for screening for HER2-positive tumors.[24] Compared with peptide macromolecules, small-molecule compounds have the advantages of being smaller in molecular weight, structurally simpler to modify, and readily available economically, with a high penetration capacity into solid tumor tissues

Received: September 26, 2025
Revised: October 23, 2025
Accepted: October 28, 2025
Published: October 31, 2025

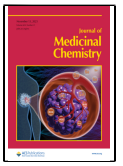

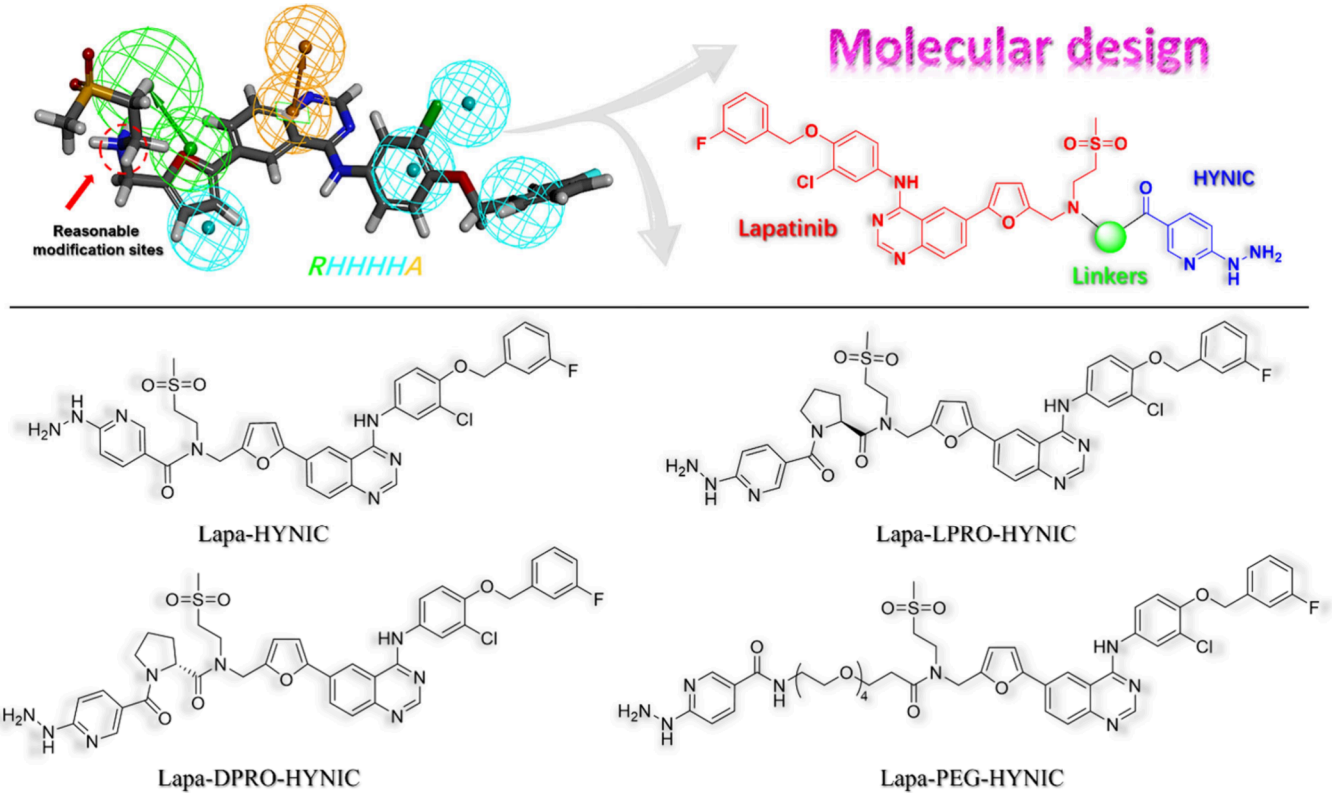

Figure 1. Molecular design and structures of HER2 precursors.

Scheme 1. Synthetic Route of HER2 Precursors[a]

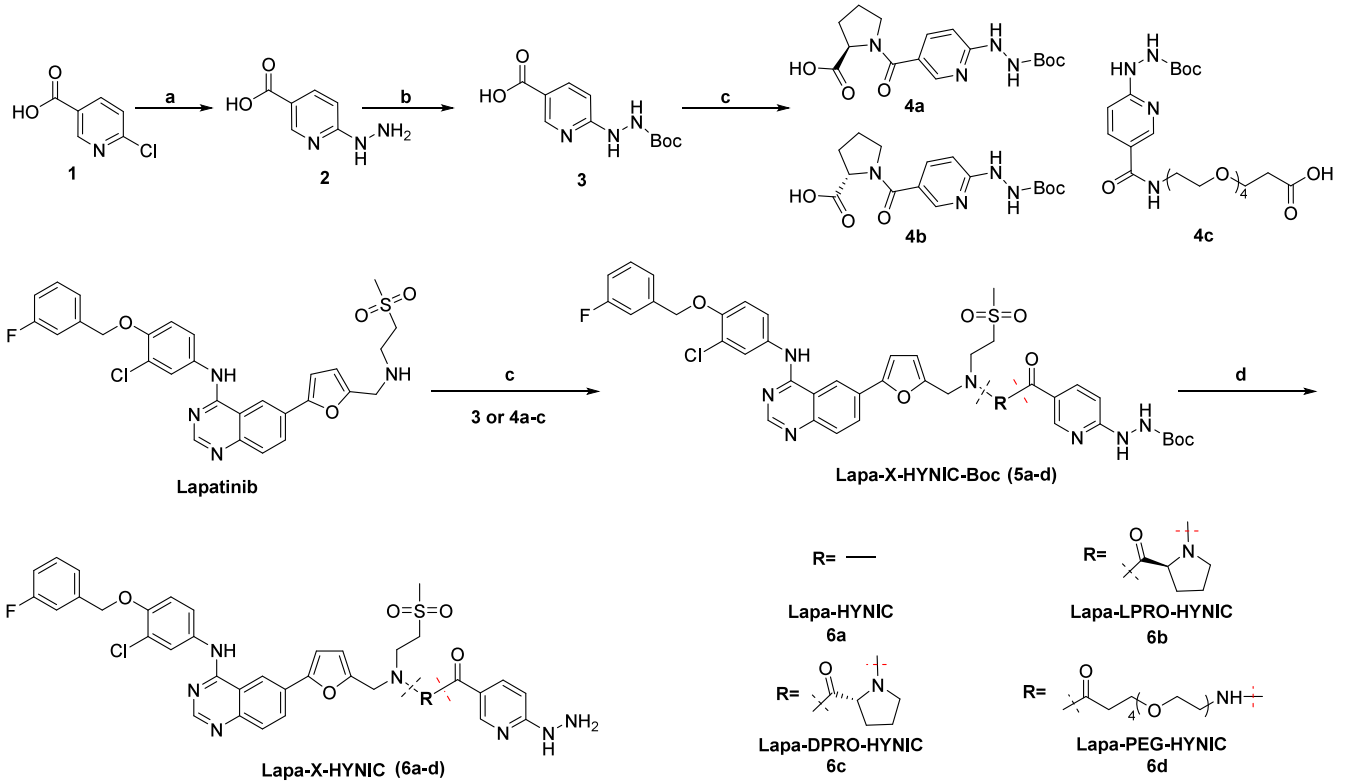

[a](a) hydrazine hydrate, H_2O,100 °C, overnight; (b) Di-tert-butyl dicarbonate, TEA, DMF, rt, 12 h; (c) HATU, TEA, DMF, rt, 12 h; (d)TFA, DMF, rt, 3 h.

https://doi.org/10.1021/acs.jmedchem.5c02789
J. Med. Chem. 2025, 68, 23620−23631

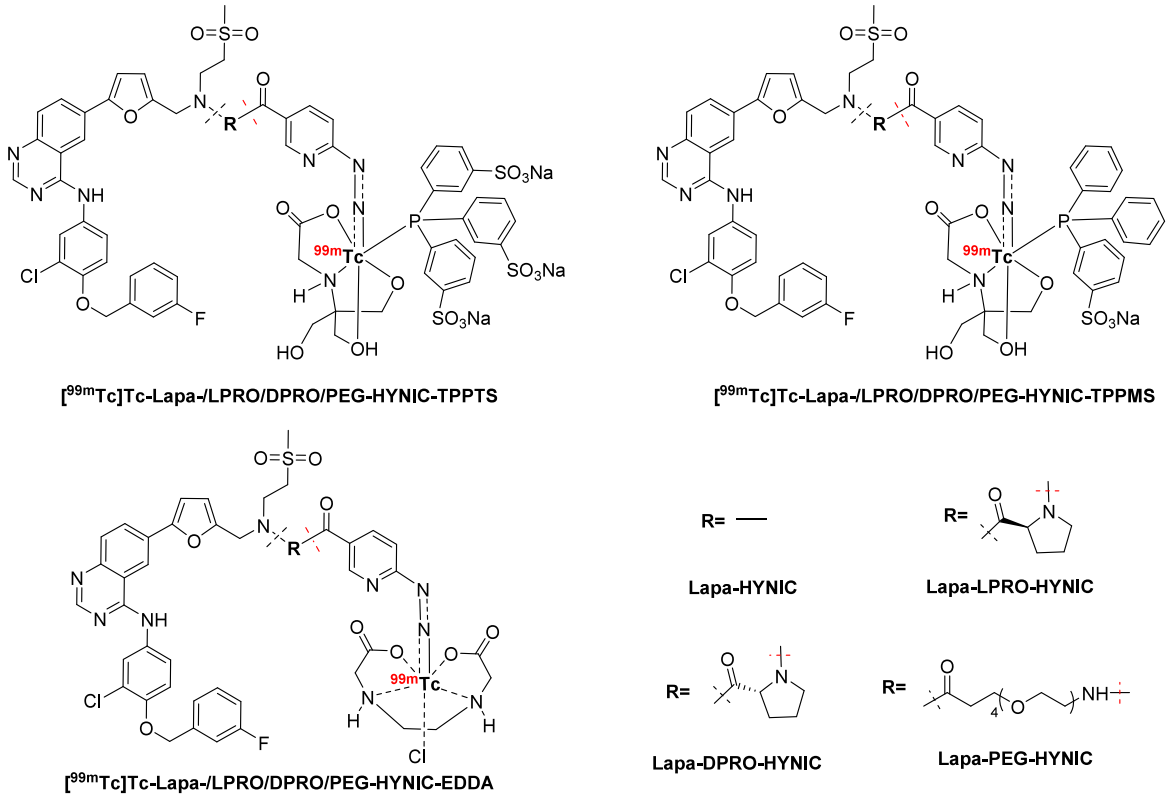

Figure 2. Speculative Structure of HER2 radiotracers.

and rapid blood clearance.[25] Lapatinib is an important member of the HER2-targeted group of drugs and plays an important role in HER2-positive breast cancer treatment, particularly in patients whose cancer has progressed beyond resistance to trastuzumab. After resistance to trastuzumab, lapatinib provides another avenue for HER2 targeting.[26] As a "universal nuclide" in the field of single-photon emission computed tomography (SPECT), ^{99m}Tc plays an important role in nuclear medicine.[27] Therefore, radiolabeling the small-molecule inhibitor lapatinib with ^{99m}Tc to develop novel targeted HER2 radiotracers is a reasonable and promising strategy.

Linkers play an important role in improving the pharmacokinetics of radiopharmaceuticals. In our previous studies of targeted prostate-specific membrane antigen (PSMA) radiotracers, we explored the effect of linker types between the target group and the radionuclide chelators on the performance of the tracer. Studies have shown that proline and hydrophilic groups such as polyethylene glycol (PEG) significantly reduce nontargeted organ uptake.[28,29] Hydrazine nicotinamide (HYNIC) is a chelator extensively studied in the chemistry of ^{99m}Tc radiopharmaceuticals.[27] Because the HYNIC group has only one coordinating atom, stable [^{99m}Tc]Tc-HYNIC requires the addition of coligands such as sodium trisulfonate (TPPTS), diphenylphosphine benzene-3-sulfonate (TPPMS), ethylenediaminetetraacetic acid (EDDA) and tricine. The rich coligand composition is important for adjusting the stability, lipophilicity and target-binding capacity of the tracers. In this study, we aimed to construct a novel ^{99m}Tc-labeled HER2-targeted SPECT tracer by rational structural modification of the target group lapatinib. To achieve this goal (Figure 1), we conducted a reasonable analysis of the lapatinib modification strategy and explored the effects of different linkers on the pharmacokinetic properties by adjusting the type of linker between HYNIC and lapatinib. Their pharmacokinetics and potential as SPECT imaging tracers after radiolabeling with ^{99m}Tc were evaluated *in vitro* and *in vivo*.

RESULTS

Molecular Design. The molecular pharmacophore properties (RHHHHA) of lapatinib were extracted from molecular common elements of pharmacodynamic models. In terms of molecular structure, quinazoline is the center of the aromatic ring (R), 2-chlorophenyl and fluorobenzene are acceptors of hydrogen bonding (A), and furan is a hydrophobic feature (H). The secondary amine is located in a nonessential position in the molecule, providing an appropriate site for lapatinib modification. The linker covalently bonds the target group to the chelator via an amide bond and successfully forms four precursors (Figure 1), namely, Lapa-HYNIC (no linker), Lapa-LPRO-HYNIC (L-proline as a linker), Lapa-DPRO-HYNIC (D-proline as a linker) and Lapa-PEG-HYNIC (PEG_4 as a linker).

Chemistry. The synthesis of HER2-targeted precursors is shown in Scheme 1. Starting with hexachloronicotinic acid, chelators containing different linkers were obtained by hydrazidation and amino preservation. In the presence of the coupling agent 2-(7-azabenzotriazol-1-yl)-*N*,*N*,*N*′,*N*′-tetramethyluronium hexafluorophosphate (HATU), lapatinib was attached to the chelators using a stable amide bond. Four target precursors were obtained by deprotection of amino-preservation, and the yields were 52.39%, 37.44%, 35.62%, and 47.98%, respectively. All the compounds were characterized by ^{1}H nuclear magnetic resonance (^{1}H NMR) and mass spectrometry (MS).

https://doi.org/10.1021/acs.jmedchem.5c02789
J. Med. Chem. 2025, 68, 23620−23631

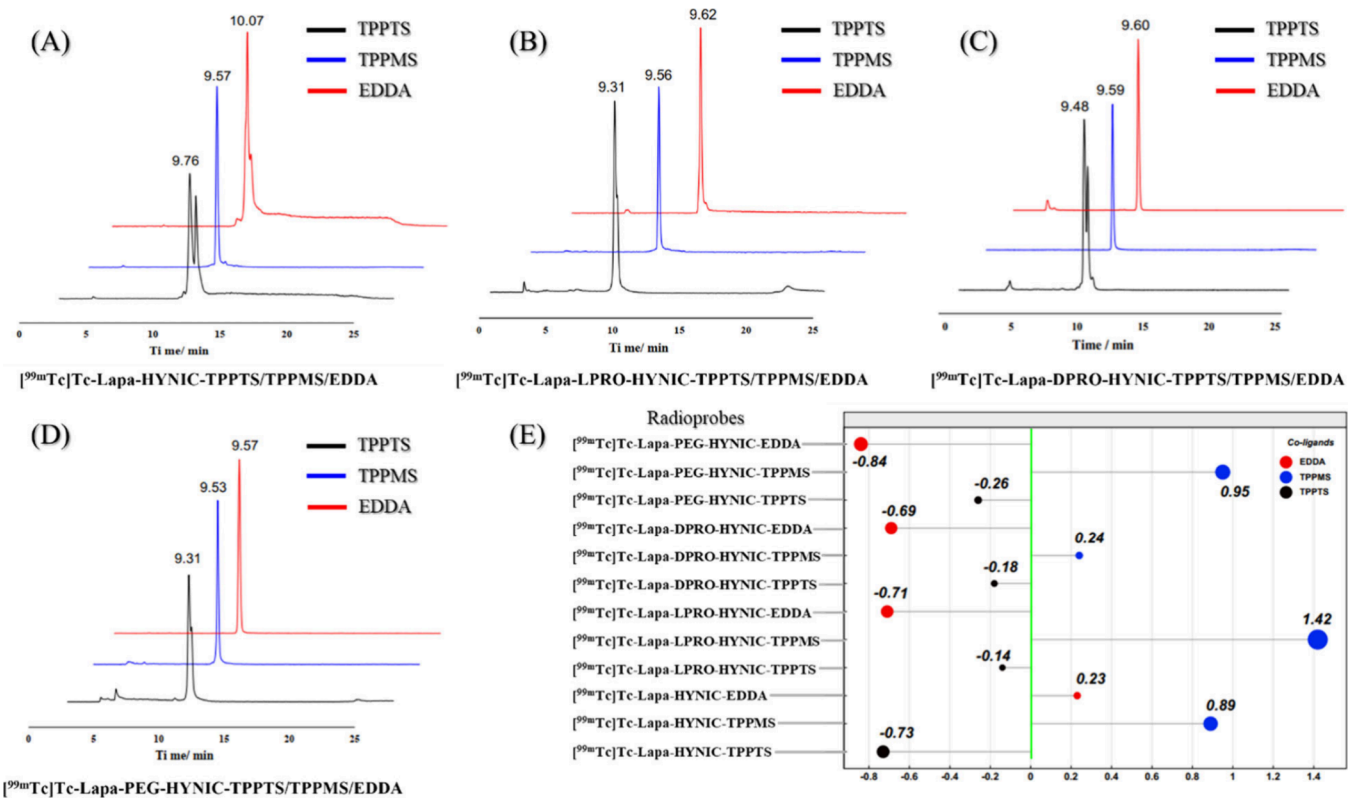

Figure 3. HPLC characterization and Log *P* of all HER2 radiotracers. (A) [^{99m}Tc]Tc-Lapa-HYNIC-TPPTS/TPPMS/EDDA; (B) [^{99m}Tc]Tc-Lapa-LPRO-HYNIC-TPPTS/TPPMS/EDDA; (C) [^{99m}Tc]Tc-Lapa-DPRO-HYNIC-TPPTS/TPPMS/EDDA; (D) [^{99m}Tc]Tc-Lapa-PEG-HYNIC-TPPTS/TPPMS/EDDA; (E) Log *P* of HER2 radiotracers.

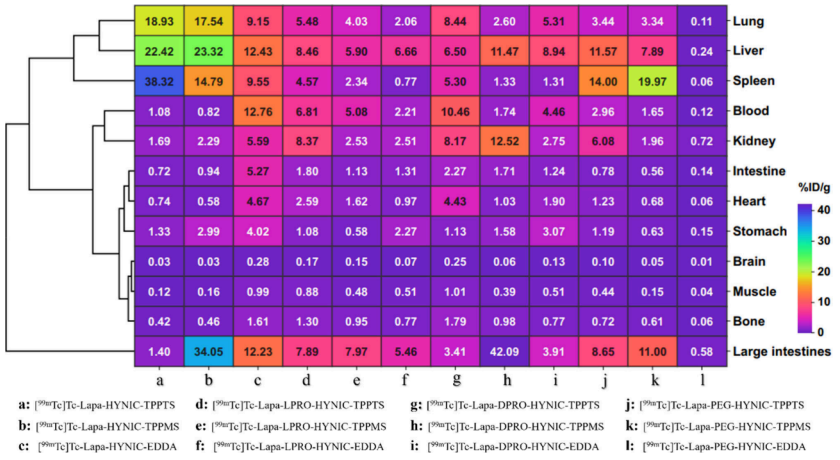

Figure 4. Biodistribution of radiotracers in normal Kunming mice (n = 5) at 2 h after injection.

Radiolabeling. As shown in Figure 2, each precursor forms 3 stable ^{99m}Tc labels with different coligands (TPPTS, TPPMS, and EDDA), resulting in a total of 12 SPECT tracers targeting HER2. The retention times for [^{99m}Tc]Tc-Lapa-HYNIC-TPPTS/TPPMS/EDDA were 9.76, 9.57, and 10.07 min, with radiochemical purities (RCP) of 98.62%, 98.36%, and 99.27%, respectively. For [^{99m}Tc]Tc-Lapa-LPRO-HYNIC-TPPTS/TPPMS/EDDA, the retention times were 9.31, 9.56, and 9.62 min, and the corresponding RCP were 97.38%, 98.55%, and 97.83%. In the case of [^{99m}Tc]Tc-Lapa-DPRO-HYNIC-TPPTS/TPPMS/EDDA, retention times of 9.48, 9.59, and 9.60 min were observed, along with RCP of 98.14%, 99.02%, and 95.78%. Finally, [^{99m}Tc]Tc-Lapa-PEG-HYNIC-TPPTS/TPPMS/EDDA showed retention times of 9.31, 9.53, and 9.57 min, with RCP of 95.42%, 97.95%, and 98.76%. The labeling process for all the radiotracers followed standardized protocols, and the entire labeling and analysis process was completed within 60 min. The RCP of all the radiotracers was greater than 95% (Figure 3A–D), and these radiotracers can be used directly in subsequent studies without further purification.

Stability and Log *P* Assessment. All the radiotracers remained significantly stable in physiological saline for up to 4 h (Figure S1). As shown in Figure 3E and Table S1, the radiotracers exhibit moderate hydrophilicity (Log *P* = 1.42 ~ −0.84), with [^{99m}Tc]Tc-Lapa-PEG-HYNIC-EDDA having the

https://doi.org/10.1021/acs.jmedchem.5c02789
J. Med. Chem. 2025, 68, 23620−23631

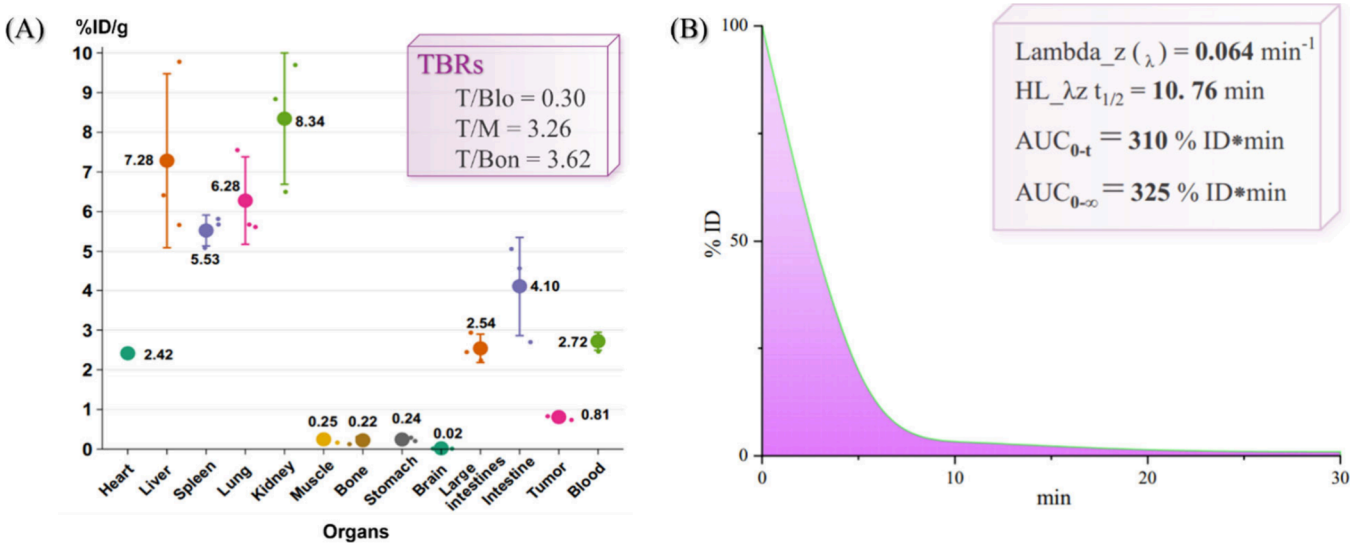

Figure 5. (A) [^{99m}Tc]Tc-Lapa-HYNIC-TPPTS biodistribution of SKBR3 tumor-bearing mice (n = 3) at 2 h after injection; (B) Blood clearance of [^{99m}Tc]Tc-Lapa-HYNIC-TPPTS in normal Kunming mice (n = 3) within 0−30 min.

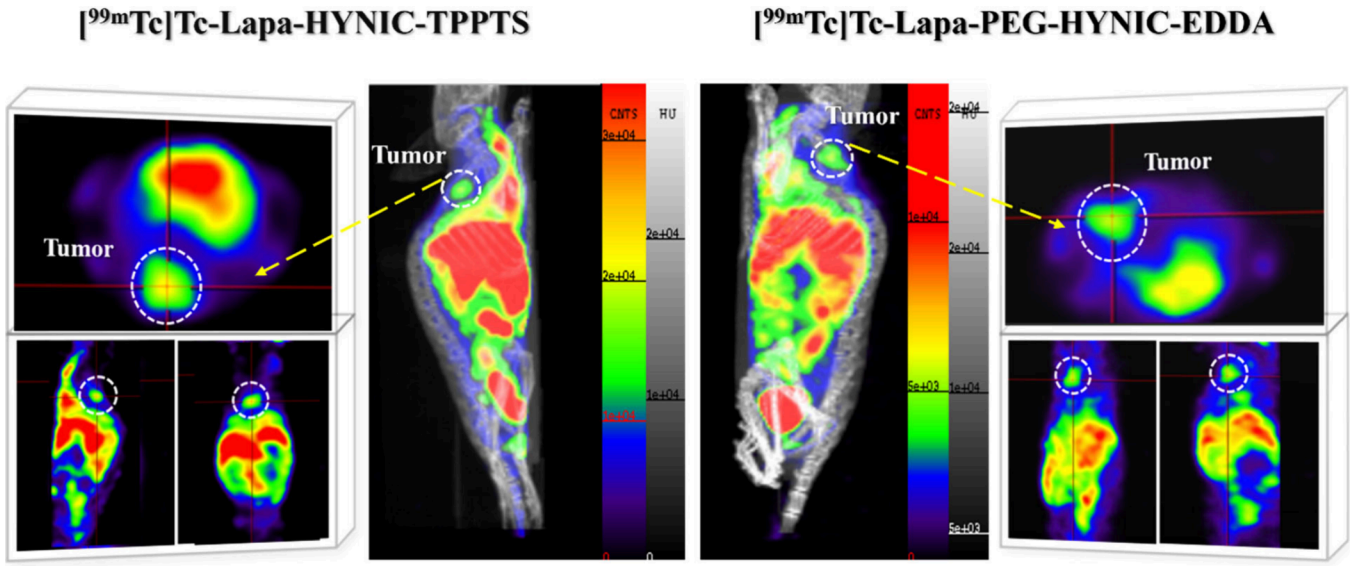

Figure 6. Micro SPECT/CT images of [^{99m}Tc]Tc-Lapa-HYNIC-TPPTS and [^{99m}Tc]Tc-Lapa-PEG-HYNIC-EDDA in SKBR3 tumor-bearing female BALB/c nude mice at 2 h after injection.

strongest hydrophilic properties (Log P = −0.84 ± 0.03) and [^{99m}Tc]Tc-Lapa-LPRO-HYNIC-TPPMS (Log P = 1.42 ± 0.01) having the strongest lipophilic properties. Interestingly, among the precursors without a linker, the coligand TPPTS is more effective than EDDA in enhancing the water solubility of radiotracers. However, for the other three precursors with a linker present, EDDA may be more effective than TPPTS.

Biodistribution Studies. Preliminary pharmacokinetic studies of all the radiotracers in normal Kunming mice are shown in Figure 4 and Tables S2−S5. A clustering analysis of the biodistribution of radiotracers in different organs revealed that the accumulation of radiotracers is greatest in the lungs and liver, followed by the large intestine and spleen. A comparison of the effects of different coligands on the clearance of radiotracers in the blood shows that their behavior may be influenced by the lipophilicity of tracers. In the Tc-Lapa-HYNIC precursor, [^{99m}Tc]Tc-Lapa-HYNIC-TPPTS has a faster blood clearance rate compared with [^{99m}Tc]Tc-Lapa-HYNIC-EDDA (1.08 ± 0.09 vs 12.76 ± 1.01% ID/g). Among the other three precursors, the coligand EDDA tracer was more effective for blood clearance compared with TPPTS (2.21 ± 0.06 vs 6.81 ± 0.23% ID/g, 4.46 ± 0.43 vs 10.46 ± 1.09% ID/g, 0.12 ± 0.01 vs 2.96 ± 0.15% ID/g, respectively). This pattern was also reflected in the kidneys. The uptake of the four radiotracers when TPPMS was used as a coligand in the large intestine was greater than that when TPPTS and EDDA were used as coligands, which may be related to higher lipophilicity. However, it should be noted that the uptake of all tracers in muscle and bone is low, which may increase the tracer tumor-to-background ratios (TBRs).

As shown in Figure 5A and Table S6, the biodistribution study of [^{99m}Tc]Tc-Lapa-HYNIC-TPPTS in SKBR3 model mice revealed that the liver (7.28 ± 1.79% ID/g) and lungs (6.28 ± 0.90% ID/g) exhibited significantly high uptake at 2 h post injection, whereas the kidneys (8.34 ± 1.35% ID/g), intestines (4.10 ± 1.02% ID/g), and spleen (5.53 ± 0.32% ID/

https://doi.org/10.1021/acs.jmedchem.5c02789
J. Med. Chem. 2025, 68, 23620−23631

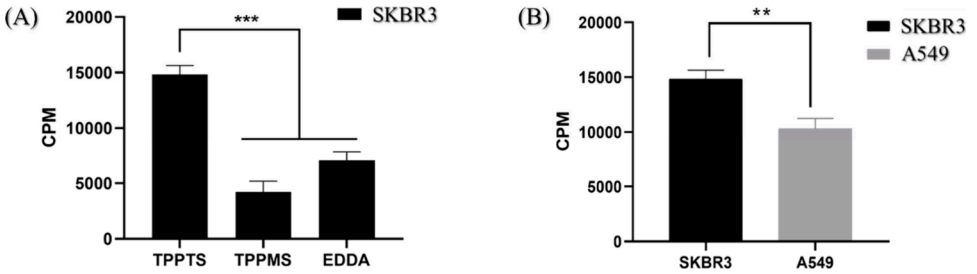

Figure 7. (A) The uptake of [^{99m}Tc]Tc-Lapa-HYNIC-TPPTS, [^{99m}Tc]Tc-Lapa-HYNIC-TPPMS and [^{99m}Tc]Tc-Lapa-HYNIC-EDDA in SKBR3 (HER2+) cells at 2 h. (B) Uptake of [^{99m}Tc] Tc-Lapa-HYNIC-TPPTS in SKBR3 (HER2+) and A549 (HER2−) cells at 2 h. $^{**}P < 0.01$, $^{***}P < 0.001$.

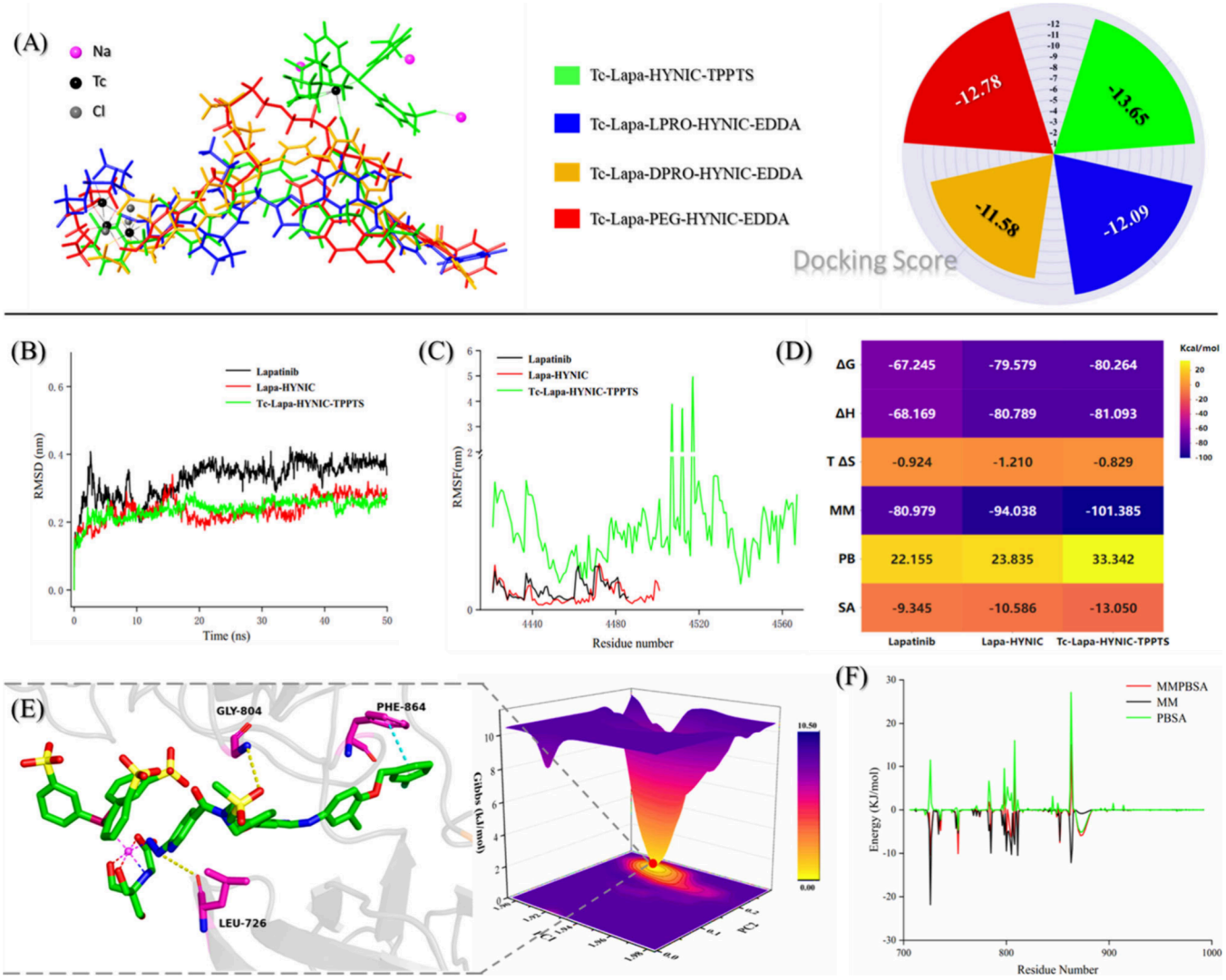

Figure 8. Molecular dynamics and docking of precursors. (A) Molecular Docking and superposition; (B) RMSD of the protein backbone; (C) RMSF of the ligands; (D) MMPBSA energy decomposition of Tc-Lapa-HYNIC-TPPTS; (E) Interactions within protein cavities; (F) Contribution of protein residues to the MMPBSA energy of Tc-Lapa-HYNIC-TPPTS.

g) also exhibited significant retention. Muscles (0.25 ± 0.06% ID/g) and bones (0.22 ± 0.07% ID/g) had lower uptake, which was consistent with observations in Kunming mice. Moreover, it was relatively highly retained in the blood (2.72 ± 0.18% ID/g) and effectively accumulated in tumors (0.81 ± 0.05% ID/g). The ratios of tumors to blood (T/Blo), tumor to muscle (T/M), and tumors to bone (T/Bon) were 0.30, 3.26, and 3.62, respectively. Further investigation of the drug metabolism performance of the tracers over time revealed that their main pharmacokinetic parameters in the blood were as follows: Lambda_z (λ) = 0.064 min^{-1}, HL_λz $t_{1/2}$ = 10.76 min, $AUC_{0\text{-}t}$ = 310% ID·min, and $AUC_{0\text{-}\infty}$ = 325% ID·min (Figure 5B).

Micro-SPECT/CT Imaging Studies. The imaging potential of the tracer was explored in SKBR3 (HER2+) and U87 (HER2−) model mice (Figures 6 and S2). SPECT/CT

https://doi.org/10.1021/acs.jmedchem.5c02789
J. Med. Chem. 2025, 68, 23620−23631

imaging of [^{99m}Tc]Tc-Lapa-HYNIC-TPPTS and [^{99m}Tc]Tc-Lapa-PEG-HYNIC-EDDA revealed that both could clearly locate the tumor 2 h after injection and significantly accumulated in the liver, lungs, intestines, and spleen. The SPECT images 4 h after injection of [^{99m}Tc]Tc-Lapa-HYNIC-TPPTS showed a decrease in uptake within the tumor, as well as a relative decrease in nontarget organ uptake (Figure S2A). The uptake of [^{99m}Tc]Tc-Lapa-LPRO-HYNIC-EDDA and [^{99m}Tc]Tc-Lapa-DPRO-HYNIC-EDDA in nontarget organs was more significant, with stronger background interference on tumor localization, resulting in less contrast in SPECT/CT images (Figure S2B,C). The biodistribution of [^{99m}Tc]Tc-Lapa-HYNIC-TPPTS was consistent with previous observations. However, a discrepancy was observed between the SPECT imaging results and the biodistribution results of the other three tracers in Kunming mice was noted, and good nontarget clearance ability was not detected. In addition, [^{99m}Tc]Tc-Lapa-HYNIC-TPPTS did not show effective tumor uptake in U87 model mice and was highly retained in nontarget organs (Figure S2D). The effective localization of the tumor by the tracer [^{99m}Tc]Tc-Lapa-HYNIC-TPPTS has shown potential in the diagnosis of HER2-positive cancers.

Cellular Uptake Studies. [^{99m}Tc]Tc-Lapa-HYNIC-TPPTS showed high affinity for HER2 in SKBR3 (HER2+) cells. As shown in Figure 7A, the uptake of [^{99m}Tc]Tc-Lapa-HYNIC-TPPMS and [^{99m}Tc]Tc-Lapa-HYNIC-EDDA into SKBR3 cells was only 28.5% and 47.7%, respectively, that of [^{99m}Tc]Tc-Lapa-HYNIC-TPPTS. In contrast, the uptake of [^{99m}Tc]Tc-Lapa-HYNIC-TPPTS by SKBR3 cells was 30.3% greater than that by A549 (HER2−) cells (Figure 7B).

Molecular Dynamics and Docking Studies. The HER2 (PDB: 7JXH) binding potency of the tracers was verified by molecular dynamics (MDs) and docking (Figure 8). The docking results of Tc-Lapa-HYNIC-TPPTS, Tc-Lapa-LPRO-HYNIC-EDDA, Tc-Lapa-DPRO-HYNIC-EDDA, and Tc-Lapa-PEG-HYNIC-EDDA with the HER2 protein reveal that all four bind within the active pocket, with docking scores of −13.65, −12.09, −11.58, and −12.78, respectively (Figures 8A and S3). Tc-Lapa-HYNIC-TPPTS and Tc-Lapa-PEG-HYNIC-EDDA seem to exhibit more favorable binding potential. The differences in binding between the Tc-Lapa-HYNIC-TPPTS and Lapa-HYNIC proteins, as well as between the Lapatinib and HER2 proteins, were further analyzed using molecular dynamics. The root-mean-square deviation (RMSD) of the protein backbone indicates the stability of the compound in the 50 ns simulation system and the reliability of the analysis results (Figure 8B). Root mean square fluctuation (RMSF) analysis revealed significant variations in the structure of the compound, which supports its close binding to the active pocket of the protein (Figure 8C). The molecular mechanics Poisson−Boltzmann surface area (MMPBSA, Figure 8D) energy calculation indicates that Tc-Lapa-HYNIC-TPPTS has a more favorable Gibbs binding energy (−80.264 vs −67.245 vs −79.579 kcal/mol). Compared with Lapatinib and Lapa-HYNIC, Tc-Lapa-HYNIC-TPPTS has more significant advantages in terms of molecular mechanics (MM, −101.385 vs −80.979 vs −94.038 kcal/mol) and nonpolar solvation energy (SA, −13.050 vs −9.345 vs −10.586 kcal/mol). As a result of its increased molecular structure, it also exhibits a significantly higher energy of polar solvation (PB, 33.342 vs 22.155 vs 23.835 kcal/mol). No obvious difference in the entropy ($T\Delta S$, −0.829 vs −0.924 vs −1.210 kcal/mol) was noted among the three radiotracers. Further analysis of the Tc-Lapa-HYNIC-TPPTS-protein complex revealed that only one of the lowest energy wells was present in the simulation system, suggesting that the protein and Tc-Lapa-HYNIC-TPPTS have a minimally stable conformation (Figure 8E). It can form stable hydrogen bond interactions with GLY804 and LEU726 and P-π interactions with PHE864. Further energy decomposition analysis revealed that these residues contribute the most to the energy contribution of the Tc-Lapa-HYNIC-TPPTS-protein complex (Figure 8F).

DISCUSSION

Lapatinib is a key member of the HER2-targeted therapy family and plays a significant role in treating HER2-positive breast cancer. Lapatinib offers an alternative pathway for continued HER2 inhibition, particularly after resistance to trastuzumab develops.[26,30] Compared with peptide macromolecules, small-molecule compounds offer several advantages, including lower molecular weight, simpler structural features, ease of chemical modification, cost effectiveness, enhanced penetration into solid tumor tissues, and rapid clearance from the bloodstream. Currently, the development of HER2-targeted radiotracers focuses primarily on radiolabeled macromolecules,[31] with comparatively less attention devoted to small-molecule inhibitors. In this study, we selected the small-molecule inhibitor lapatinib as the targeting group. On the basis of the results of the pharmacophore analysis, we identified suitable sites for molecular modification, optimized the linker between the targeting group and the chelator, and adjusted the composition of the coligands. Subsequently, 12 stable ^{99m}Tc-labeled HER2-targeting tracers were designed and prepared. The [^{99m}Tc]Tc-Lapa-HYNIC-TPPTS and [^{99m}Tc]-Tc-Lapa-DPRO-HYNIC-TPPTS exhibit double peaks in the HPLC chromatogram, which can be attributed to isomerism arising from the [^{99m}Tc]Tc-HYNIC core.[32] The ^{99m}Tc labeling method is simple, the radionuclide source is convenient, and the 12 stable tracers can be used directly without purification (RCP > 90%), which is easy to promote and clinically apply.

All the radiotracers demonstrated good stability under *in vitro* conditions, with no observable degradation after 4 h of incubation in physiological saline, exhibiting moderate hydrophilicity (Log P = 1.42 ∼ −0.84). Among them, [^{99m}Tc]Tc-Lapa-PEG-HYNIC-EDDA was the most hydrophilic (Log P = -0.84 ± 0.03), followed by [^{99m}Tc]Tc-Lapa-HYNIC-TPPTS (Log P = −0.73 ± 0.01). The use of coligands is an effective strategy for modulating the lipophilicity of radiotracers. Comparative studies have demonstrated that compared with those incorporating TPPMS, TPPTS and EDDA coligands significantly increase the hydrophilicity of the resulting tracers. Interestingly, for the precursor without a linker (Lapa-HYNIC), the coligand TPPTS confers greater water solubility to the tracer than EDDA does. In contrast, compared with TPPTS, EDDA appears to be more effective at enhancing the hydrophilicity of the other three precursors that contain linkers. When the relationship between Log P and the structure of the radiotracers is analyzed, it is evident that no strict linear correlation exists between these parameters. It can be inferred that the modulation of lipophilicity is not merely the result of additive contributions from individual functional groups but also depends on the synergistic effects arising from the overall molecular architecture.

Preliminary pharmacokinetic evaluation of all the radiotracers was performed in normal Kunming mice. The results indicated high uptake in the lungs and liver across all tracers,

https://doi.org/10.1021/acs.jmedchem.5c02789
J. Med. Chem. 2025, 68, 23620−23631

followed by the large intestine and spleen. Lower accumulation was observed in the muscle, bone, stomach, and heart, whereas moderate uptake levels were noted in the blood and kidneys. A comparison of the pharmacokinetic effects of radiotracers with those of different linkers revealed that compared with linker-free (Lapa-HYNIC) tracers, the introduction of L-proline, D-proline, and PEG chains significantly reduced tracer accumulation in highly retentive organs (such as the liver and lung). These results demonstrate that rational modification of the linker represents an effective strategy for tuning the pharmacokinetics of radiotracers. Among the linker-free tracers, [^{99m}Tc]Tc-Lapa-HYNIC-TPPTS demonstrated faster blood clearance compared with [^{99m}Tc]Tc-Lapa-HYNIC-EDDA (1.08 ± 0.09 vs 12.76 ± 1.01% ID/g). In contrast, among the three precursors featuring a linker, the EDDA-based tracers are more efficient than their TPPTS counterparts—a trend that is also reflected in kidney clearance. This observation aligns with the trends identified in the lipophilicity studies, suggesting that lipid−water distribution is a key determinant of the pharmacokinetics of the tracers. These results further validate that modulating the coligand composition represents a rational and feasible strategy for optimizing the metabolic profile of radiotracers, which is consistent with our initial design approach. [^{99m}Tc]Tc-Lapa-HYNIC-EDDA has the highest blood retention among all tracers. In addition to the influence of the coligand, the solubility of the molecule may also be an important factor. Although Tween 80 was added to enhance molecular solubility, its administration may lead to increased adsorption upon entering the bloodstream. The high uptake of [^{99m}Tc]Tc-Lapa-DPRO-HYNIC-TPPTS in the blood may also be related to this factor. Compared with those with TPPTS or EDDA, the four radiotracers with TPPMS as the coligand exhibit greater large intestine uptake, which is potentially attributed to their greater lipophilicity. Encouragingly, all the tracers demonstrated low uptake in muscle and bone (approximately 1% ID/g), a characteristic that holds significant potential for improving TBRs. Preliminary pharmacokinetic evaluation revealed that [^{99m}Tc]Tc-Lapa-HYNIC-TPPTS, [^{99m}Tc]Tc-Lapa-LPRO-HYNIC-EDDA, [^{99m}Tc]Tc-Lapa-DPRO-HYNIC-EDDA, and [^{99m}Tc]Tc-Lapa-PEG-HYNIC-EDDA exhibit favorable biodistribution properties. These candidates have therefore been selected as lead tracers for SPECT/CT imaging studies.

As a HER2-overexpressing cell line, SKBR3 was used to establish tumor-bearing mouse models that were widely employed in the biological assessment of HER2 tracers.[33,34] [^{99m}Tc]Tc-Lapa-HYNIC-TPPTS exhibited optimal SPECT/CT imaging performance in the SKBR3 (HER2+) tumor-bearing mouse model, with clear tumor localization observed within 2 h postinjection. Tracer accumulation was also detected in the liver, lungs, intestines, and spleen, which is consistent with the biodistribution previously observed in Kunming mice. The SPECT/CT imaging results of [^{99m}Tc]Tc-Lapa-LPRO-HYNIC-EDDA, [^{99m}Tc]Tc-Lapa-DPRO-HYNIC-EDDA, and [^{99m}Tc]Tc-Lapa-PEG-HYNIC-EDDA revealed notable deviations in biodistribution in Kunming mice. Significant accumulation was observed in nontargeted organs such as the liver, lungs, intestines, and spleen. In particular, [^{99m}Tc]Tc-Lapa-LPRO-HYNIC-EDDA and [^{99m}Tc]Tc-Lapa-DPRO-HYNIC-EDDA exhibited more pronounced background interference, which considerably affected tumor localization clarity. [^{99m}Tc]Tc-Lapa-PEG-HYNIC-EDDA has imaging potential similar to that of [^{99m}Tc]Tc-Lapa-HYNIC-TPPTS, effectively achieving tumor localization and high uptake in nontarget organs. The significant discrepancies observed in both SPECT/CT imaging and biodistribution results are intriguing, and molecular docking results offer a plausible explanation for these findings. Tc-Lapa-HYNIC-TPPTS seems to exhibit more favorable HER2 protein binding potential compared with Tc-Lapa-LPRO-HYNIC-EDDA, Tc-Lapa-DPRO-HYNIC-EDDA, and Tc-Lapa-PEG-HYNIC-EDDA (docking scores: −13.65 vs −12.09, −11.58, and −12.78, respectively). Insufficient affinity for the HER2 protein may lead to reduced tumor uptake, thereby significantly diminishing SPECT image contrast. Furthermore, another reason for the differences in preliminary pharmacokinetic studies and SPECT imaging may be due to differences between mouse species. The differences in biodistribution of the same tracer in different mouse-derived organs was evident, which can also be observed in the research of PSMA-targeting tracers.[28,29] The SPECT imaging of [^{99m}Tc]Tc-Lapa-HYNIC-TPPTS delayed to 4 h showed a trend of reduction in highly accumulated organs such as liver and lung compared to 2 h, at the same time, the accumulation within the tumor was also relatively cleared, but still effectively localizing the tumor. As a HER2 negative cell line,[35] [^{99m}Tc]Tc-Lapa-HYNIC-TPPTS also exhibited high uptake in nontarget organs such as the liver in tumor-bearing mice of U87, but no significant retention was observed in the tumors. The differential uptake of [^{99m}Tc]Tc-Lapa-HYNIC-TPPTS in the SKBR3 (HER2+) and U87 (HER2−) mouse models demonstrated its high specificity for HER2.

The biodistribution of [^{99m}Tc]Tc-Lapa-HYNIC-TPPTS was also evaluated in SKBR3 tumor-bearing mice. At 2 h postinjection, consistent with the SPECT/CT imaging findings, significant uptake was observed in the liver (7.28 ± 1.79% ID/g), lungs (6.28 ± 0.90% ID/g), intestines (4.10 ± 1.02% ID/g), and spleen (5.53 ± 0.32% ID/g), with the highest uptake occurring in the kidneys (8.34 ± 1.35% ID/g) and moderate uptake occurring in the blood (2.72 ± 0.18% ID/g). The phenomenon of high retention in organs such as liver, kidney, and lung may be common in HER2 tracer studies, such as the ^{99m}Tc-labeled small molecule peptide tracer [^{99m}Tc]Tc-(CGGG)-LTVSPWY (Liver, 13.62 ± 5.32% ID/g; Lung, 9.46 ± 2.82% ID/g; Kidney, 76.61 ± 5.77% ID/g; 1 h),[33] the ^{11}C-labeled small molecule inhibitor [^{11}C]tucatinib (Liver, 9.83 ± 1.65% ID/g; Kidney, 5.39 ± 0.07% ID/g; 1 h),[23] and the ^{99m}Tc-labeled monoclonal antibody tracer [^{99m}Tc]Tc-NM-02, which also exhibit high accumulation in human liver and kidney.[36] The emergence of this phenomenon may be a common challenge in the development of such tracers, and modifying their metabolic pathways could be an important strategy for future tracer optimization. Notably, effective tracer accumulation (0.81 ± 0.05% ID/g) was also confirmed at the tumor site. Moreover, uptake in bone and muscle remained low, with TBRs of 3.62 (T/Bon), 3.26 (T/M), and 0.30 (T/Blo), respectively. Further investigation of the blood pharmacokinetics of [^{99m}Tc]Tc-Lapa-HYNIC-TPPTS revealed a terminal elimination rate constant (Lambda_z (λ)) of 0.064 min^{-1} and a terminal elimination half-life (HL_λz $t_{1/2}$) of 10.76 min. The area under the blood concentration−time curve ($AUC_{0\text{-}t}$) was 310% ID·min compared with a theoretical ($AUC_{0\text{-}\infty}$) of 325% ID·min. The relatively slow blood clearance rate leads to prolonged

https://doi.org/10.1021/acs.jmedchem.5c02789
J. Med. Chem. 2025, 68, 23620−23631

retention of [^{99m}Tc]Tc-Lapa-HYNIC-TPPTS in the circulation.

As a characterized HER2-negative cell line, A549 is essential for the bioevaluation of novel HER2 tracers.[37] [^{99m}Tc]Tc-Lapa-HYNIC-TPPTS also showed high affinity for HER2 in SKBR3 (HER2+) and A549 (HER2−) cells. The uptake of [^{99m}Tc]Tc-Lapa-HYNIC-TPPTS was 30.3% greater in SKBR3 cells than in A549 cells, demonstrating its ability to selectively target HER2 in cells with differential HER2 expression. When the effects of different coligands on cellular uptake were evaluated, [^{99m}Tc]Tc-Lapa-HYNIC-TPPTS demonstrated the most favorable performance, with a 71.5% increase compared with [^{99m}Tc]Tc-Lapa-HYNIC-TPPMS and a 52.3% increase relative to [^{99m}Tc]Tc-Lapa-HYNIC-EDDA. To further elucidate the mechanism of action of [^{99m}Tc]Tc-Lapa-HYNIC-TPPTS, MDs were performed. The RMSD of the protein backbone indicates the stability of the compound within the 50 ns simulation system and the reliability of the analysis results. Unlike the positive molecule Lapatinib and the precursor Lapa-HYNIC, the RMSF of the coligand part (TPPTS) in Tc-Lapa-HYNIC-TPPTS is relatively significant, indicating tight binding between TPPTS and the protein active pocket. It forms stable hydrogen bonds with the LEU726 residue, which is identified as one of the key energy-contributing amino acids facilitating the formation of the stable Tc-Lapa-HYNIC-TPPTS−protein complex. The MMPBSA energy calculations reveal that compared with both Lapatinib and Lapa-HYNIC, Tc-Lapa-HYNIC-TPPTS exhibits a more favorable Gibbs binding energy (−80.264 vs −67.245, −79.579 kcal/mol), with significant improvements in MM (−101.385 vs −80.979, −94.038 kcal/mol) and SA (−13.050 vs −9.345, −10.586 kcal/mol). This means that it can form more favorable interactions within the active pocket, including mainly stable hydrogen bond interactions with GLY804 and LEU726, as well as P-π interactions with PHE864. Further energy decomposition analysis confirms that these residues constitute key contributors to the Gibbs free energy. Tc-Lapa-HYNIC-TPPTS has a slightly unfavorable PB (33.342 vs 22.155, 23.835 kcal/mol). Compared with Lapatinib and Lapa-HYNIC, its larger molecular structure leads to more pronounced solvation effects. However, no significant differences in entropy (TΔS, −0.829 vs −0.924, −1.210 kcal/mol) were observed among the three compounds, suggesting that the macromolecular structure of Tc-Lapa-HYNIC-TPPTS retains considerable conformational flexibility. This property is conducive to inducing the formation of stable protein complexes. MDs provided a theoretical basis for the binding behavior of Tc-Lapa-HYNIC-TPPTS to the HER2 protein, further confirming its good binding affinity.

CONCLUSIONS

In this study, we selected small-molecule HER2 inhibitors as target groups and L-proline, D-proline and PEG chains as linkers to design and synthesize 4 precursors that can be used to label [^{99m}Tc]Tc-HYNIC. Twelve stable radiotracers have been prepared by combining ^{99m}Tc with various coligands. All the tracers were stable and were subjected to preliminary pharmacokinetic studies. [^{99m}Tc]Tc-Lapa-HYNIC-TPPTS exhibits the most favorable pharmacokinetic properties, as it can stably bind to the active cavity of the HER2 protein, and a difference in tumor uptake in cells and SPECT imaging suggests that it effectively targets HER2. [^{99m}Tc]Tc-Lapa-HYNIC-TPPTS exhibits high potential for the diagnosis of HER2-positive cancers, as it can be effectively located within the tumor. Low uptake in muscle and bone results in good TBRs. This study represents the first attempt to develop a ^{99m}Tc-labeled small-molecule inhibitor tracer targeting HER2, which complements diagnostic tracers targeting HER2 intracellular targets. [^{99m}Tc]Tc-Lapa-HYNIC-TPPTS is expected to provide a powerful tool for the classification of HER2 status in breast cancer patients, monitoring treatment efficacy, and assessing resistance.

EXPERIMENTAL SECTION

General. Unless otherwise stated, all reactions were performed in flame-dried glassware under a nitrogen atmosphere with magnetic stirring. All reagents were obtained from Tong Guang Fine Chemicals Company (Beijing, China), Aladdin, Innochem, and J&K. ^{1}H NMR spectra were recorded on a JNM-ECS spectrometer (JEOL, Tokyo, Japan) operating at 400 or 600 MHz. Chemical shifts are reported relative to tetramethylsilane (TMS) as an internal standard or to residual solvent peaks. Coupling constants (J) are expressed in hertz (Hz). MS data were acquired using electrospray ionization (ESI) on a Thermo Scientific LCQ mass spectrometer (Thermo, USA). Radioactive high-performance liquid chromatography (R-HPLC) analyses were conducted using a Shimadzu 20A system (Shimadzu, Kyoto, Japan) equipped with a Kromasil C18 column (250 × 4.6 mm, 5 μm). Saline was used to elute [^{99m}Tc]$NaTcO_4$ from a ^{99} Mo/^{99m}Tc generator purchased from Zhibo Bio-Medical Technology (Beijing, China). Radioactivity was measured with a Wizard 2480 γ-counter (PerkinElmer, Singapore). The SKBR3 and A549 cell lines were obtained from the Typical Culture Collection of the Chinese Academy of Sciences (Beijing, China). *In vivo* imaging studies were performed using a micro-SPECT/CT system (Trifoil, CA). MDs were performed on a high-performance computing system equipped with a 44-core/88-thread CPU, 128 GB of RAM, and an RTX 2080 Ti GPU (22 GB), running on Ubuntu 22.04.2.

Radiolabeling. *[^{99m}Tc]Tc-Lapa-HYNIC-TPPTS.* Tricine (1 mg), TPPTS (2 mg) and Tween 80 (500 μg) were dissolved in 0.5 mL of phosphate-buffered saline (PBS). To this mixture, succinate buffer adjusted to a pH of 5.5 was added (0.3 mL), followed by Lapa-HYNIC (10 μg) and 0.5 mL of freshly eluted [^{99m}Tc]$NaTcO_4$ (37−370 MBq) in sequence, and the mixture was then subjected to a reaction at 100 °C for 30 min to yield the radiotracer [^{99m}Tc]Tc-Lapa-HYNIC-TPPTS.

[^{99m}Tc]Tc-Lapa-HYNIC-TPPMS. Tricine (1 mg), TPPMS (2 mg) and Tween 80 (500 μg) were dissolved in 0.5 mL of PBS. To this mixture, succinate buffer adjusted to a pH of 5.5 was added (0.3 mL), followed by Lapa-HYNIC (10 μg) and 0.5 mL of freshly eluted [^{99m}Tc]$NaTcO_4$ (37−370 MBq) in sequence, and the mixture was then subjected to a reaction at 100 °C for 30 min to yield the radiotracer [^{99m}Tc]Tc-Lapa-HYNIC-TPPMS.

[^{99m}Tc]Tc-Lapa-HYNIC-EDDA. Tricine (20 mg), EDDA (10 mg) and Tween 80 (500 μg) were dissolved in 0.5 mL of PBS. To this solution, succinate buffer adjusted to a pH of 7.5 was added (0.2 mL), the solution pH was adjusted to 7.0−8.0 with NaOH (1 mol/L), followed by Lapa-HYNIC (10 μg), $SnCl_2{\cdot}2H_2O$ (100 μg) and 0.5 mL of freshly eluted [^{99m}Tc]$NaTcO_4$ (37−370 MBq) in sequence, and the mixture was then subjected to a reaction at 100 °C for 20 min to yield the radiotracer [^{99m}Tc]Tc-Lapa-HYNIC-EDDA.

The preparation methods for the other three labeled precursor tracers are identical to that of Lapa-HYNIC, except that the corresponding labeled precursors need to be substituted. The RCP of all the radiotracers has been verified by RHPLC to be greater than 95%, and these radiotracers can be used directly in subsequent studies without further purification.

R-HPLC Analysis and Stability Assay. The RCP and *in vitro* stability of the ^{99m}Tc-labeled radiotracers were analyzed by R-HPLC using a Shimadzu 20A system equipped with a Kromasil C18 column (250 × 4.6 mm, 5 μm). The mobile phase consisted of water containing 0.1% trifluoroacetic acid (TFA) as phase A and acetonitrile

https://doi.org/10.1021/acs.jmedchem.5c02789
J. Med. Chem. 2025, 68, 23620−23631

as phase B. The injection volume was 10 μL, and the flow rate was maintained at 1.0 mL/min. The gradient elution program was set as follows: 10% B (0−2 min), increased linearly from 10% to 90% B (2−5 min), held at 90% B (5−20 min), and then returned linearly to 10% B (20−25 min). To evaluate the stability in saline, the radiolabeled solution was stored at 37 °C for 4 h, after which R-HPLC was performed to determine the RCP.

Octanol/Water Partition Coefficient (Log *P*). The Log *P* values of the radiotracers were determined using the shake flask method. Prior to the experiment, the *n*-octanol was presaturated by equilibrating it overnight with phosphate-buffered saline (PBS; 0.025 mol/L, pH 7.4). Briefly, 900 μL of PBS, 1 mL of presaturated *n*-octanol, and 100 μL of radiotracer were combined in a centrifuge tube and vigorously shaken for 5 min. The mixture was then centrifuged at 10,000 rpm for 15 min to achieve phase separation. Subsequently, 500 μL aliquots from both the PBS and *n*-octanol phases were collected, and their radioactivity was measured using a γ-counter. The distribution coefficient was calculated on the basis of the radioactivity counts in each phase and is expressed as Log *P* = log (cpm in *n*-octanol/cpm in PBS). The results were derived from three independent parallel experiments and are presented as the mean ± SD.

Cell Culture and Tumour Models. The cancer cell lines SKBR3 (HER2+) and A549 (HER2−) were cultured in 1640 supplemented with 10% (v/v) heat-inactivated FBS (fetal bovine serum) and 1% (v/v) penicillin streptomycin at 37 °C in a cell culture incubator with 5% CO_2.

All mice were purchased from Shibeifu Experimental Animal Company (Beijing, China). Initial pharmacokinetic studies were conducted using female Kunming mice (4−5 weeks old). For biodistribution and SPECT imaging studies, a SKBR3 tumor-bearing model was established by subcutaneously inoculating female BALB/c nude mice (4−5 weeks old) with 100 μL of SKBR3 cell suspension (approximately 1×10^7 cells) behind the right ear. Experiments were performed 3 weeks after inoculation, at which time the tumor diameter had reached approximately 5−12 mm.

All animals were raised in a pathogen-free 26 °C environment with ample space for movement, socialization, and natural behaviors. They had continuous access to clean water and a balanced feed. All of the animal protocols were approved and supervised by the Institutional Animal Care and Use Committee of Beijing Normal University (permit no. BNUCC-EAW-2022001).

Biodistribution Studies in Mice. In the initial pharmacokinetic study of all the radiotracers, Kunming mice (n = 5) were utilized for evaluation. Each mouse was administered a ^{99m}Tc-labeled tracer (1.85 ± 0.05 MBq, 100 μL) via tail vein injection and euthanized 2 h postinjection. Blood and major organs—including the heart, liver, spleen, lungs, kidneys, muscle, bone, stomach, brain, large intestine, and small intestine—were collected, weighed, and measured for radioactivity using a γ-counter. A biodistribution study was conducted in the SKBR3 tumor-bearing mouse model (n = 3) following the same experimental procedure. The results are expressed as the percentage of injected doses per gram of organ or tissue (%ID/g) and are reported as the mean ± SD. Additionally, blood samples were collected from Kunming mice at 0, 5, 15, and 30 min after tracer administration, and their radioactivity was quantified with a γ-counter. Pharmacokinetic parameters were derived by fitting a noncompartmental model to the blood radioactivity−time profile using Phoenix software.

Cellular Uptake. SKBR3 and A549 cells were seeded in 24-well plates (1×10^5 cells per well) and incubated overnight. Each well was then treated with 0.5 mL of fresh culture medium containing the ^{99m}Tc-labeled tracer (0.37 MBq). After 2 h of incubation, the medium was aspirated, and the cells were washed twice with cold PBS. The cells were subsequently lysed using 1 M NaOH. Radioactivity in the lysates was quantified using a γ-counter.

Small Animal Micro-SPECT/CT Imaging. Radiotracers (37 MBq, 100 μL) were intravenously administered to SKBR3 and U87 tumor-bearing mice. Prior to imaging, the mice were anaesthetized with 3% (v/v) isoflurane. SPECT/CT scans were performed at 2 h postinjection under maintenance anesthesia with 1.5% isoflurane delivered in the air at a flow rate of 500 mL/min. Image postprocessing was conducted using VivoQuant 2.4 software.

Molecular Docking and Dynamics Assay. A pharmacophore model of lapatinib was generated using the structure-based pharmacophore module in Discovery Studio. The resulting model comprises five key pharmacophoric features: a hydrogen bond donor (D), a hydrogen bond acceptor (B), a hydrophobic/aromatic center (H), ionic interaction sites (P), and an aromatic ring plane (R). The molecular docking studies were performed using AutoDock 4.2. The receptor structure was obtained from the Protein Data Bank (PDB ID: 7JXH). The target molecule was first optimized in Gaussian 09 using the Amber 99 force field to generate the three-dimensional structure for docking. The cocrystallized ligand was used to define the docking center, and the binding site was considered unrestricted under default parameter settings. The initial docking poses were further subjected to MDs using Gromacs 2020. The GAFF force field was applied for small molecule parametrization, while the Amber99SB force field was used for the protein. The SPC water model was employed for solvation. Systems underwent energy minimization followed by NVT and NPT equilibration for 2 ns each, and production MDs were performed for 50 ns. The stability of the simulations was assessed by analyzing the RMSD and RMSF. Binding free energy calculations were performed using the MMPBSA method on the last 10 ns of the trajectory. The final representative conformation was visualized and analyzed using PyMOL.

■ ASSOCIATED CONTENT

Supporting Information

The Supporting Information is available free of charge at https://pubs.acs.org/doi/10.1021/acs.jmedchem.5c02789.

Molecular formula strings (CSV)

Supporting Information for synthesis of precursor, Supporting Information for radiotracer stability and Log *P*, Supporting Information for biodistribution, micro-SPECT/CT imaging, molecular dynamics, ^{1}H NMR and MS spectra (PDF)

The interaction between the HER2 and Tc-Lapa-LPRO-HYNIC-EDDA (PDB)

The interaction between the HER2 and Tc-Lapa-HYNIC-TPPTS (PDB)

The interaction between the HER2 and Tc-Lapa-DPRO-HYNIC-EDDA (PDB)

The interaction between the HER2 and Tc-Lapa-PEG-HYNIC-EDDA (PDB)

■ AUTHOR INFORMATION

Corresponding Authors

Jianyong Jiang − *Key Laboratory of Beam Technology of the Ministry of Education, College of Physics and Astronomy, Beijing Normal University, Beijing 100875, P. R. China*; Email: jianyong@bnu.edu.cn

Junbo Zhang − *Key Laboratory of Radiopharmaceuticals of the Ministry of Education, College of Chemistry, NMPA Key Laboratory for Research and Evaluation of Radiopharmaceuticals (National Medical Products Administration), Beijing Normal University, Beijing 100875, P. R. China*; orcid.org/0000-0003-3549-6483; Email: zhjunbo@bnu.edu.cn

Authors

Zuojie Li − *Key Laboratory of Radiopharmaceuticals of the Ministry of Education, College of Chemistry, NMPA Key Laboratory for Research and Evaluation of Radiopharmaceuticals (National Medical Products*

Administration), Beijing Normal University, Beijing 100875, P. R. China; Key Laboratory of Beam Technology of the Ministry of Education, College of Physics and Astronomy, Beijing Normal University, Beijing 100875, P. R. China

Lina Diao − *Key Laboratory of Radiopharmaceuticals of the Ministry of Education, College of Chemistry, NMPA Key Laboratory for Research and Evaluation of Radiopharmaceuticals (National Medical Products Administration), Beijing Normal University, Beijing 100875, P. R. China*

Peiwen Han − *Key Laboratory of Radiopharmaceuticals of the Ministry of Education, College of Chemistry, NMPA Key Laboratory for Research and Evaluation of Radiopharmaceuticals (National Medical Products Administration), Beijing Normal University, Beijing 100875, P. R. China*

Qingna Xiao − *Key Laboratory of Radiopharmaceuticals of the Ministry of Education, College of Chemistry, NMPA Key Laboratory for Research and Evaluation of Radiopharmaceuticals (National Medical Products Administration), Beijing Normal University, Beijing 100875, P. R. China*

Dajie Ding − *Key Laboratory of Radiopharmaceuticals of the Ministry of Education, College of Chemistry, NMPA Key Laboratory for Research and Evaluation of Radiopharmaceuticals (National Medical Products Administration), Beijing Normal University, Beijing 100875, P. R. China*

Junhong Feng − *Key Laboratory of Radiopharmaceuticals of the Ministry of Education, College of Chemistry, NMPA Key Laboratory for Research and Evaluation of Radiopharmaceuticals (National Medical Products Administration), Beijing Normal University, Beijing 100875, P. R. China*

Complete contact information is available at: https://pubs.acs.org/10.1021/acs.jmedchem.5c02789

Notes

The authors declare no competing financial interest.

■ ACKNOWLEDGMENTS

This work was financially supported, in part, by the National Natural Science Foundation of China (22076013, 22276015), the Beijing Natural Science Foundation (2232010) and the Beijing Nova Program (20230484470).

■ ABBREVIATIONS

EDDA, ethylenediaminediacetic acid; HATU, 2-(7-azabenzotriazol-1-yl)-*N,N,N′,N′*-tetramethyluronium hexafluorophosphate; HER2, human epidermal growth factor receptor 2; HYNIC, hydrazinonicotinamide; MDs, Molecular dynamics; MM, molecular mechanics energy; MMPBSA, molecular mechanicspoisson-boltzmann surface area; MS, Mass spectra; NMR, nuclear magnetic resonance; PB, polar solvation energy; PBS, phosphate buffered saline; PDB, protein data bank; PEG, polyethylene glycol; PSMA, prostate-specific membrane antigen; RCP, radiochemical purity; R-HPLC, radioactive high-performance liquid chromatography; RMSD, root-mean-square deviation; RMSF, root-mean-square fluctuation; SA, nonpolar solvation energy; SPECT, single photon emission computed tomography; TBRs, tumor-to-background ratios; TPPTS, triphenylphosphine trisulfonate; TPPMS, diphenylphosphine benzene-3-sulfonate; ΔS, entropy

■ REFERENCES

(1) Arteaga, C. L.; Sliwkowski, M. X.; Osborne, C. K.; Perez, E. A.; Puglisi, F.; Gianni, L. Treatment of HER2-Positive Breast Cancer: Current Status and Future Perspectives. *Nat. Rev. Clin Oncol* **2012**, *9* (1), 16−32.

(2) Loibl, S.; Gianni, L. HER2-Positive Breast Cancer. *Lancet* **2017**, *389* (10087), 2415−2429.

(3) Oh, D. Y.; Bang, Y. J. HER2-Targeted Therapies - a Role Beyond Breast Cancer. *Nat. Rev. Clin Oncol* **2020**, *17* (1), 33−48.

(4) Cheng, X. A Comprehensive Review of HER2 in Cancer Biology and Therapeutics. *Genes* **2024**, *15* (7), 903−917.

(5) Waks, A. G.; Martínez-Sáez, O.; Tarantino, P.; Braso-Maristany, F.; Pascual, T.; Cortés, J.; Tolaney, S. M.; Prat, A. Dual HER2 Inhibition: Mechanisms of Synergy, Patient Selection, and Resistance. *Nat. Rev. Clin Oncol* **2024**, *21* (11), 818−832.

(6) Loibl, S.; Poortmans, P.; Morrow, M.; Denkert, C.; Curigliano, G. Breast Cancer. *Lancet* **2021**, *397* (10286), 1750−1769.

(7) Friedlaender, A.; Subbiah, V.; Russo, A.; Banna, G. L.; Malapelle, U.; Rolfo, C.; Addeo, A. EGFR and HER2 Exon 20 Insertions in Solid Tumours: From Biology to Treatment. *Nat. Rev. Clin Oncol* **2022**, *19* (1), 51−69.

(8) Marchiò, C.; Annaratone, L.; Marques, A.; Casorzo, L.; Berrino, E.; Sapino, A. Evolving Concepts in HER2 Evaluation in Breast Cancer: Heterogeneity, HER2-Low Carcinomas and Beyond. *Semin Cancer Biol.* **2021**, *72*, 123−135.

(9) Ahuja, S.; Khan, A. A.; Zaheer, S. Understanding the Spectrum of HER2 Status in Breast Cancer: From HER2-Positive to Ultra-Low HER2. *Pathol Res. Pract* **2024**, *262*, No. 155550.

(10) Wolff, A. C.; Somerfield, M. R.; Dowsett, M.; Hammond, M. E. H.; Hayes, D. F.; McShane, L. M.; Saphner, T. J.; Spears, P. A.; Allison, K. H. Human Epidermal Growth Factor Receptor 2 Testing in Breast Cancer: Asco-College of American Pathologists Guideline Update. *J. Clin Oncol* **2023**, *41* (22), 3867−3872.

(11) Galogre, M.; Rodin, D.; Pyatnitskiy, M.; Mackelprang, M.; Koman, I. A Review of HER2 Overexpression and Somatic Mutations in Cancers. *Crit Rev. Oncol Hematol* **2023**, *186*, No. 103997.

(12) Nützinger, J.; Bum Lee, J.; Li Low, J.; Ling Chia, P.; Talisa Wijaya, S.; Chul Cho, B.; Min Lim, S.; Soo, R. A. Management of HER2 Alterations in Non-Small Cell Lung Cancer-the Past, Present, and Future. *Lung cancer* **2023**, *186*, No. 107385.

(13) Agostinetto, E.; Curigliano, G.; Piccart, M. Emerging Treatments in HER2-Positive Advanced Breast Cancer: Keep Raising the Bar. *Cell reports. Medicine* **2024**, *5* (6), No. 101575.

(14) Krishnamurti, U.; Silverman, J. F. HER2 in Breast Cancer: A Review and Update. *Adv. Anat Pathol* **2014**, *21* (2), 100−107.

(15) Grassini, D.; Cascardi, E.; Sarotto, I.; Annaratone, L.; Sapino, A.; Berrino, E.; Marchiò, C. Unusual Patterns of HER2 Expression in Breast Cancer: Insights and Perspectives. *Pathobiology* **2022**, *89* (5), 278−296.

(16) Joshi, S. S.; Badgwell, B. D. Current Treatment and Recent Progress in Gastric Cancer. *CA Cancer J. Clin* **2021**, *71* (3), 264−279.

(17) Hong, R.; Xu, B. Breast Cancer: An up-to-Date Review and Future Perspectives. *Cancer Commun. (Lond)* **2022**, *42* (10), 913−936.

(18) Dehdashti, F.; Wu, N.; Bose, R.; Naughton, M. J.; Ma, C. X.; Marquez-Nostra, B. V.; Diebolder, P.; Mpoy, C.; Rogers, B. E.; Lapi, S. E.; et al. Evaluation of [^{89}Zr]Trastuzumab-PET/CT in Differentiating HER2-Positive from HER2-Negative Breast Cancer. *Breast Cancer Res. Treat* **2018**, *169* (3), 523−530.

(19) Laforest, R.; Lapi, S. E.; Oyama, R.; Bose, R.; Tabchy, A.; Marquez-Nostra, B. V.; Burkemper, J.; Wright, B. D.; Frye, J.; Frye, S.; et al. [^{89}Zr]Trastuzumab: Evaluation of Radiation Dosimetry, Safety, and Optimal Imaging Parameters in Women with HER2-Positive Breast Cancer. *Mol. Imaging Biol.* **2016**, *18* (6), 952−959.

(20) Xavier, C.; Vaneycken, I.; D'Huyvetter, M.; Heemskerk, J.; Keyaerts, M.; Vincke, C.; Devoogdt, N.; Muyldermans, S.; Lahoutte,

T.; Caveliers, V. Synthesis, Preclinical Validation, Dosimetry, and Toxicity of ^{68}Ga-NoTA-Anti-HER2 Nanobodies for PET Imaging of HER2 Receptor Expression in Cancer. *J. Nucl. Med.* **2013**, *54* (5), 776−784.
(21) Garousi, J.; Lindbo, S.; Nilvebrant, J.; Åstrand, M.; Buijs, J.; Sandström, M.; Honarvar, H.; Orlova, A.; Tolmachev, V.; Hober, S. Adapt, a Novel Scaffold Protein-Based Probe for Radionuclide Imaging of Molecular Targets That Are Expressed in Disseminated Cancers. *Cancer Res.* **2015**, *75* (20), 4364−4371.
(22) Shi, J.; Du, S.; Wang, R.; Gao, H.; Luo, Q.; Hou, G.; Zhou, Y.; Zhu, Z.; Wang, F. Molecular Imaging of HER2 Expression in Breast Cancer Patients Using a Novel Peptide-Based Tracer ^{99m}Tc-HP-Ark2: A Pilot Study. *J. Transl Med.* **2023**, *21* (1), 19−35.
(23) Müller, M.; Shalgunov, V.; Hvass, L.; Jørgensen, J. T.; Kramer, V.; Staudt, M.; Battisti, U. M.; Kjaer, A.; Herth, M. M. Synthesis and *in vivo* Evaluation of [^{11}C]Tucatinib for HER2-Targeted PET Imaging. *Bioorg. Med. Chem. Lett.* **2023**, *80*, No. 129088.
(24) Ge, S.; Li, J.; Yu, Y.; Chen, Z.; Yang, Y.; Zhu, L.; Sang, S.; Deng, S. Review: Radionuclide Molecular Imaging Targeting HER2 in Breast Cancer with a Focus on Molecular Probes into Clinical Trials and Small Peptides. *Molecules* **2021**, *26* (21), 6482−6495.
(25) Li, Z.; Ruan, Q.; Jiang, Y.; Wang, Q.; Yin, G.; Feng, J.; Zhang, J. Current Status and Perspectives of Novel Radiopharmaceuticals with Heterologous Dual-Targeted Functions: 2013−2023. *J. Med. Chem.* **2024**, *67* (24), 21644−21670.
(26) Yuan, Y.; Liu, X.; Cai, Y.; Li, W. Lapatinib and Lapatinib Plus Trastuzumab Therapy Versus Trastuzumab Therapy for HER2 Positive Breast Cancer Patients: An Updated Systematic Review and Meta-Analysis. *Syst. rev* **2022**, *11* (1), 264−293.
(27) Duatti, A. Review on ^{99m}Tc Radiopharmaceuticals with Emphasis on New Advancements. *Nucl. Med. Biol.* **2021**, *92*, 202−216.
(28) Li, Z.; Duan, X.; Han, P.; Yin, G.; Jiang, Y.; Ruan, Q.; Zhang, J. Synthesis and Evaluation of ^{99m}Tc-Labelled L-Aspartic Acid as a Euk Polymer Linker for Targeting PSMA to a Novel SPECT Tumour Tracer. *J. Med. Chem.* **2024**, *67* (23), 21617−21628.
(29) Li, Z.; Jiang, Y.; Ruan, Q.; Yin, G.; Han, P.; Duan, X.; Zhang, J. Synthesis and Evaluation of ^{99m}Tc-Labelled $_{D}$Pro-Gly-Containing Tracers Targeting PSMA. *Mol. Pharmaceutics* **2024**, *21* (10), 5305−5314.
(30) Bilancia, D.; Rosati, G.; Dinota, A.; Germano, D.; Romano, R.; Manzione, L. Lapatinib in Breast Cancer. *Ann. Oncol* **2007**, *18* (Suppl 6), vi26−30.
(31) Miladinova, D. Molecular Imaging of HER2 Receptor: Targeting HER2 for Imaging and Therapy in Nuclear Medicine. *Front Mol. Biosci* **2023**, *10*, No. 1144817.
(32) Torabizadeh, S. A.; Hosseinimehr, S. J. The Influence of Co-Ligands on Improving Tumor Targeting of ^{99m}Tc-HYNIC Conjugated Peptides. *Mini Rev. Med. Chem.* **2016**, *17* (2), 86−94.
(33) Sabahnoo, H.; Noaparast, Z.; Abedi, S. M.; Hosseinimehr, S. J. New Small ^{99m}Tc-Labeled Peptides for HER2 Receptor Imaging. *Eur. J. Med. Chem.* **2017**, *127*, 1012−1024.
(34) Yadav, S. A.; Vats, V. K.; Gupta, S.; Repaka, K. M.; Satpati, D. ^{99m}Tc-HYNIC PEGylated Peptide Probe Targeting HER2-Expression in Breast Cancer. *Chem. Biol. Drug Des* **2025**, *105* (2), No. e70064.
(35) Wang, Y.; Xia, B.; Cao, L.; Yang, J.; Feng, C.; Jiang, F.; Li, C.; Gu, L.; Yang, Y.; Tian, J.; et al. Preclinical Studies of BB-1701, a HER2-Targeting Eribulin-Containing ADC With Potent Bystander Effect and ICD Activity. *Antib Ther.* **2024**, *7* (3), 221−232.
(36) Zhao, L.; Liu, C.; Xing, Y.; He, J.; O'Doherty, J.; Huang, W.; Zhao, J. Development of a ^{99m}Tc-Labeled Single-Domain Antibody for SPECT/CT Assessment of HER2 Expression in Breast Cancer. *Mol. Pharmaceutics* **2021**, *18* (9), 3616−3622.
(37) Ebrahimi, F.; Noaparast, Z.; Hosseinimehr, S. J. Evaluation of Homodimer ^{99m}Tc-HYNIC-E(SSSLTVPWY)$_2$ Peptide on HER2-over Expressed Breast Cancer Cells. *Med. Chem. Res.* **2023**, *32* (6), 1178−1189.

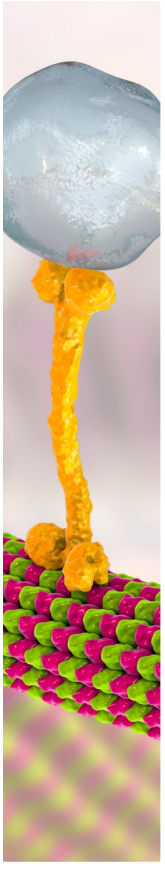

https://doi.org/10.1021/acs.jmedchem.5c02789
J. Med. Chem. 2025, 68, 23620−23631